Radiology: Imaging Cancer

REVIEW

Head and Neck Paragangliomas: An Update on the Molecular Classification, State-of-the-Art Imaging, and Management Recommendations

Edward P. Lin, MD, MBA • Bennett B. Chin, MD • Lauren Fishbein, MD, PhD • Toshio Moritani, MD, PhD • Simone P. Montoya, MD • Shehanaz Ellika, MD • Shawn Newlands, MD, PhD, MBA

From the Departments of Imaging Sciences (E.P.L., S.E.) and Otolaryngology (S.N.), University of Rochester Medical Center, 601 Elmwood Ave, Box 648, Rochester, NY 14642; Departments of Radiology (B.B.C.) and Medicine (L.F.), University of Colorado School of Medicine, Denver, Colo; Department of Radiology, University of Michigan, Ann Arbor, Mich (T.M.); Eastern Radiologists, East Carolina University, Vidant Medical Center, Greenville, NC (S.P.M.); and Department of Radiology, Massachusetts General Hospital, Boston, Mass (S.P.M.). Received August 4, 2021; revision requested October 29; revision received January 11, 2022; accepted March 24. **Address correspondence to** E.P.L. (email: *edward_lin@urmc.rochester.edu*).

Authors declared no funding for this work.

Conflicts of interest are listed at the end of this article.

Radiology: Imaging Cancer 2022; 4(3):e210088 • https://doi.org/10.1148/rycan.210088 • Content codes: HN MI OI

Paragangliomas are neuroendocrine tumors that derive from paraganglia of the autonomic nervous system, with the majority of parasympathetic paragangliomas arising in the head and neck. More than one-third of all paragangliomas are hereditary, reflecting the strong genetic predisposition of these tumors. The molecular basis of paragangliomas has been investigated extensively in the past couple of decades, leading to the discovery of several molecular clusters and more than 20 well-characterized driver genes (somatic and hereditary), which are more than are known for any other endocrine tumor. Head and neck paragangliomas are largely related to the pseudohypoxia cluster and have been previously excluded from most molecular profiling studies. This review article introduces the molecular classification of paragangliomas, with a focus on head and neck paragangliomas, and discusses its impact on the management of these tumors. Genetic testing is now recommended for all patients with paragangliomas to provide screening and surveillance recommendations for patients and relatives. While CT and MRI provide excellent anatomic characterization of paragangliomas, gallium 68 tetraazacyclododecane tetraacetic acid–octreotate (ie, ^{68}Ga-DOTATATE) has superior sensitivity and is recommended as first-line imaging in patients with head and neck paragangliomas with concern for multifocal and metastatic disease, patients with known multifocal and metastatic disease, and in candidates for targeted peptide-receptor therapy.

© RSNA, 2022

Paragangliomas (PGLs) are hypervascular neuroendocrine tumors arising from paraganglia. Paraganglia derive embryologically from neural crest cells and contain chief cells that are associated with the autonomic nervous system. Pheochromocytomas (PCCs) are neuroendocrine tumors originating from the adrenal medulla, whereas extra-adrenal PGLs (EAPGLs) originate from paraganglia outside of the adrenal gland. PCCs and EAPGLs are collectively abbreviated as PPGLs in this article and have a reported incidence of 2–8 cases per million people (1,2).

PPGLs have a strong genetic predilection. Forty percent contain germline pathogenic variants in known susceptibility genes, several of which carry an increased risk for multifocal disease or metastasis. Approximately 30% of PPGLs have somatic driver mutations (3–5). Patients with metastasis, either from hereditary or sporadic disease, have a 50% 5-year survival rate (6). The Endocrine Society 2014 and North American Neuroendocrine Tumor 2021 guidelines recommend genetic counseling and testing in all patients with PPGL (4).

While the inherited syndromes associated with PPGLs are well-known, the molecular basis of PGLs is still being uncovered, leading to an evolving molecular classification (7,8). This molecular classification has substantially improved our understanding of how genetic alterations lead to PPGLs and which mutations are associated with an increased risk for head and neck PGLs (HNPGLs), multifocal disease, and metastasis. Identifying high-risk features in patients with PPGLs should prompt further functional imaging with somatostatin receptor (SSTR) analogs, such as gallium 68 (^{68}Ga) tetraazacyclododecane tetraacetic acid –octreotate (DOTATATE) PET/CT. Therapeutic SSTR analogs are proving to be novel treatment options for patients with SSTR imaging–positive PPGLs who have locally unresectable or metastatic disease.

This review provides an update to the molecular classification of PPGLs and its impact on the management recommendations of these tumors. As prior articles have illustrated imaging characteristics on conventional anatomic imaging, this review will focus more on the recent advances in anatomic and functional imaging and treatment of HNPGLs.

Overview, Types, and Features of PGLs

Terminology

The anatomic location, not secretory function, dictates the specific name of a PGL, such as a carotid body PGL or PGL tympanicum. Previously used terms, including chemodectoma and glomus, should be avoided. Chemodectoma was first introduced by Mulligan (9) to describe tumors arising from chemoreceptors of the heart in dogs. Chemoreceptors, such as in the carotid and aortic bodies, detect and respond to changes in arterial oxygen, carbon dioxide, and pH. Because not all PGLs arise from chemoreceptor paraganglia, chemodectoma is not an inclu-

This copy is for personal use only. To order printed copies, contact reprints@rsna.org

Abbreviations

AJCC = American Joint Committee on Cancer, DCE = dynamic contrast enhanced, DOPA = dihydroxyphenylalanine, DOTATATE = tetraazacyclododecane tetraacetic acid octreotate, DOTATOC = Tyr3-octreotide, EAPGL = extra-adrenal PGL, FDA = Food and Drug Administration, FDG = fluorodeoxyglucose, HNPGL = head and neck PGL, MIBG = metaiodobenzylguanidine, MRA = MR angiography, PCC = pheochromocytoma, PGL = paraganglioma, PPGL = PCCs and EAPGLs (inclusive of all PGLs), SSTR = somatostatin receptor, TCGA = The Cancer Genome Atlas, WHO = World Health Organization

Summary

Paragangliomas (PGLs) may carry underlying hereditary pathogenic variants that are associated with increased risk for multifocal and metastatic disease, indicating the need for genetic testing in all patients with PGLs, and tumors in those cases are best assessed by gallium 68 somatostatin receptor imaging.

Essentials

- Pheochromocytomas and paragangliomas (PGLs) are neuroendocrine tumors that are often genetically driven, with an evolving molecular classification that currently identifies several molecular clusters: pseudohypoxia, kinase-signaling, Wnt altered.
- Head and neck PGLs are predominantly associated with the pseudohypoxia cluster and germline succinate dehydrogenase *(SDH)* subunit D and *SDHB* mutations, which carry an increased risk for multifocal primary disease and metastatic disease, respectively, indicating the need for genetic counseling and testing for all patients with PGLs.
- Gallium 68 somatostatin receptor imaging has superior sensitivity over all other cross-sectional and functional imaging modalities in helping detect PGLs and is recommended for patients with head and neck PGLs with concern for multifocal or metastatic disease, as well as candidates for targeted peptide-receptor therapy.

Keywords

Molecular Imaging, MR Perfusion, MR Spectroscopy, Neuro-Oncology, PET/CT, SPECT/CT, Head/Neck, Genetic Defects

sive description for all PGLs. A glomus tumor more accurately arises from the arteriovenous glomus body of the dermis, which is involved in thermoregulation and is completely unrelated to PGLs. PGL is, therefore, a more inclusive and accurate term that describes all EAPGLs by location.

Clinical Presentation and Secretory Function

Age and sex predilection are affected by whether PPGLs are sporadic or hereditary. PPGLs can occur at any age, but the majority manifest between the 3rd and 6th decades. Hereditary forms account for up to 40% of patients (3,4,10). Hereditary PPGLs manifest in earlier age groups, including pediatric populations (11–13). While some studies report a similar incidence of PPGLs among males and females, others suggest an overall female predominance (12,14). HNPGLs manifest slightly later and have a strong female predilection (15).

Most sympathetic PPGLs contain chromaffin cells and are often functional, secreting catecholamines (Fig 1). Sympathetic PPGLs are typically found in the adrenal gland, extra-adrenal abdomen and pelvis, and, less commonly, chest. Sympathetic HNPGLs exist but are uncommon (<4%). Patients with functional sympathetic PPGLs may present with a classic triad of diaphoresis, headaches and palpitations, and hypertension, but many do not. If these PPGLs are left untreated, patients can experience heart attacks, arrhythmias, and stroke.

The majority of parasympathetic PGLs are nonfunctional (Fig 1). These tumors are found predominantly in the head and neck, and, less commonly, chest or other locations. HNPGLs commonly manifest as a painless mass. A bruit may suggest compression of the carotid arteries. Lower cranial neuropathies, resulting in a hoarse voice, dysphagia, shoulder weakness, or Horner syndrome, may reflect skull base involvement or compression of cranial nerves. Skull base or middle ear invasion may also lead to hearing loss, pulsatile tinnitus, aural fullness, vertigo, or headaches.

HNPGL Characteristics

HNPGLs arise predominantly along branches of the glossopharyngeal nerve (cranial nerve IX) and vagus nerve (cranial nerve X), most commonly in the carotid body, followed by the middle ear, jugular foramen, ganglion nodosum, larynx, and cervical sympathetic chain (16). Less common locations include the pharynx, nasal fossa, paranasal sinuses, orbits, cavernous sinus, pterygopalatine fossa, thyroid, and hypoglossal nerve (16).

Anatomic location, vessel displacement, and skull base involvement allow accurate diagnosis of HNPGL type. Carotid body PGLs arise at the carotid bifurcation and splay the internal and external carotid arteries as the tumors enlarge. The Shamblin classification predicts resectability and risk of blood loss with resection of carotid body PGLs depending on the degree of vascular encasement and adhesion to the vessel wall, ranging from minimal attachment (I) to partial encasement (II), complete encasement (III), and vessel wall infiltration (IIIb) (17,18). The Shamblin classification may be predicted preoperatively by measuring the degree of internal carotid artery to tumor contact at cross-sectional imaging, with less than 180° for group I, 180–270° for group II, and greater than 270° for group III (18).

Vagal PGLs occur anywhere along the vagus nerve but most commonly arise from the ganglion nodosum or plexiform ganglion, which are located below the skull base but above and medial to the carotid bifurcation. Vagal PGLs displace the internal carotid artery anteromedially and jugular vein posterolaterally. When large, they can extend to the carotid bifurcation and invade the skull base. The Netterville-Glasscock classification categorizes vagal PGLs by degree of skull base involvement, with group A confined to the neck, group B extending to the jugular foramen, and group C invading beyond the jugular foramen (19).

Jugular foramen and jugulotympanic PGLs typically invade the skull base, with the former centered within the jugular foramen and the latter around the inferior tympanic canaliculus. PGL tympanicum are located along the cochlear promontory.

Histopathologic Analysis

PPGLs range from gray-white to pink-tan in color and are firm, ovoid masses with rubbery consistency. They consist of chief cells that grow in nests, or zellballen ("ball of cells"), of

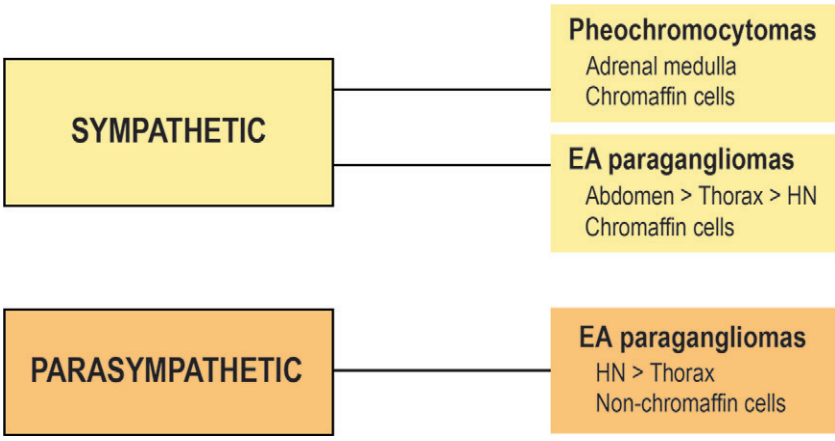


Figure 1: Overview of pheochromocytomas and paragangliomas by function, location, and cellular type. EA = extra-adrenal, HN = head and neck. (Reprinted, with permission, from University of Rochester, Rochester, New York © 2022; illustration by Nazdezhda D. Kiriyak.)

various sizes (20) (Fig 2). Chief cells, which stain positive with synaptophysin, are epithelioid and amphophilic to pink on hematoxylin-eosin staining, with round, hyperchromatic nuclei. Spindled sustentacular cells surround and provide structural support to chief cells and can be delineated by S100 and chromogranin staining. All PPGLs can exhibit cellular pleomorphism, mitotic figures, and occasionally, necrosis, as well as irregular margins to the adjacent bone and soft tissues. Glandular cells and mucin production are noticeably absent. Metastatic PPGLs are indistinguishable histopathologically from nonmetastatic PPGLs and are defined instead by the presence of distant metastases.

World Health Organization and American Joint Committee on Cancer Classifications

The World Health Organization (WHO) fourth edition (2017) (21) and American Joint Committee on Cancer (AJCC) eighth edition (2017) (22) have different aims, the former of which provides an overview of PGLs and the latter of which focuses on TNM staging. Both define PCCs as arising from the adrenal medulla and all other PGLs as EAPGLs.

The WHO fourth edition defines PCC, EAPGL, and metastatic disease, as well as describing the most common locations, clinical presentation, pathologic features, prognosis, and genetics (21). WHO describes that most parasympathetic PGLs localize to the head and neck, whereas sympathetic PGLs can be located anywhere from the skull base to pelvis. "Benign" and "malignant" terms are no longer recommended by WHO, as all PPGLs have metastatic potential. Metastatic PPGLs are defined by identifying PPGL tissue in nonparaganglia tissue.

The AJCC eighth edition focuses on defining TNM staging for PPGLs for the first time. AJCC does not use the WHO terms of localized and metastatic PPGL but rather uses the older terms, benign or malignant, the latter of which means the tumor has metastasized. HNPGLs are considered by the AJCC to be benign and are not included in TNM staging. It should be noted, however, that HNPGLs can and do metastasize in a subset of cases. Prognostic staging by the AJCC focuses on size, location, and metastasis. Although the AJCC definitions have discrepancies with what is accepted in the field, it is advantageous to include PPGL for the first time in a staging schema, allowing collection of data for future studies.

Metastatic Disease

Distant metastases of PPGL are most commonly found in the liver, lungs, bones, and lymph nodes. Metastases occur in up to 25% of PPGLs and almost twice as frequently in EAPGLs compared with PCCs (23). Metastases can occur at any time, from initial manifestation to many years following primary tumor resection, as some cases have occurred even 20 years after initial diagnosis (23). A 50% 5-year survival rate has been reported in patients with metastasis (23), with approximately half carrying the *succinate dehydrogenase (SDH)* subunit B mutation (24). Hereditary PPGLs have an overall increased risk for multifocality and, for some susceptibility genes, an increased risk for metastasis. Other risk factors for metastasis include extra-adrenal location and larger tumor size.

Molecular Classification

Genetics play a strong role in PPGL pathogenesis. The Cancer Genome Atlas (TCGA) program has identified at least 21 well-characterized driver genes, more than any other endocrine tumor (8,25). Several inherited genetic syndromes are associated with PPGLs and account for 40% of cases. Inherited pathogenic variants have been detected in 15 genes (3). Germline and somatic mutations comprise 40% and 30% of PPGL mutations, respectively.

Several molecular clusters have been described on the most recent comprehensive genomic profiling from TCGA that may have clinical implications: pseudohypoxia, kinase-signaling, and Wnt-altered (Figs 3, 4) (8). Originating from parasympathetic paraganglia, HNPGLs have been largely excluded from molecular profiling studies, which have focused on PPGLs arising from sympathetic ganglia. HNPGLs are predominantly associated with the pseudohypoxia cluster.

Pseudohypoxia cluster.— The pseudohypoxia cluster was first discovered through microarray classifications of PPGLs and has been confirmed in subsequent studies including TCGA (7,8). This cluster gives rise to nonfunctional and noradrenergic PPGLs, and most HNPGLs are thought to be included in this cluster. Noradrenergic secretion results from hypermethylation and silencing of the phenylethanolamine N-methyltransferase *(PNMT)* gene, which encodes the enzyme converting norepinephrine to epinephrine (26,27). These tumors tend to show global hypermethylation, which is associated with more aggressive clinical phenotypes (8,26).

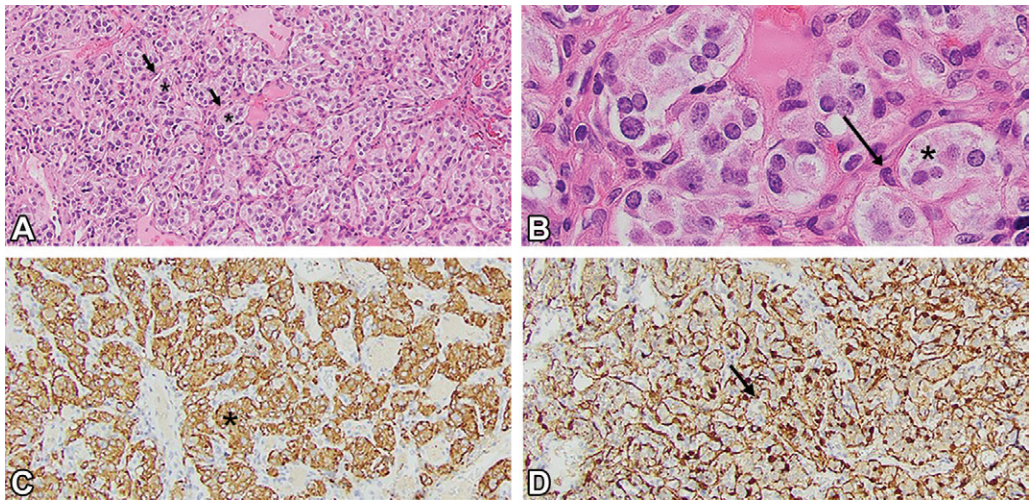


Figure 2: Histopathologic analysis. **(A, B)** Type I chief cells in well-defined nests (* = zellballen) surrounded by type II sustentacular cells (arrows). (Hematoxylin-eosin stain; original magnification, **[A]** ×10 and **[B]** ×40.) **(C)** Type I chief cells (*). (Synaptophysin stain; original magnification, ×10.) **(D)** Type II sustentacular cells (arrow). (S100 stain; original magnification, ×10.)

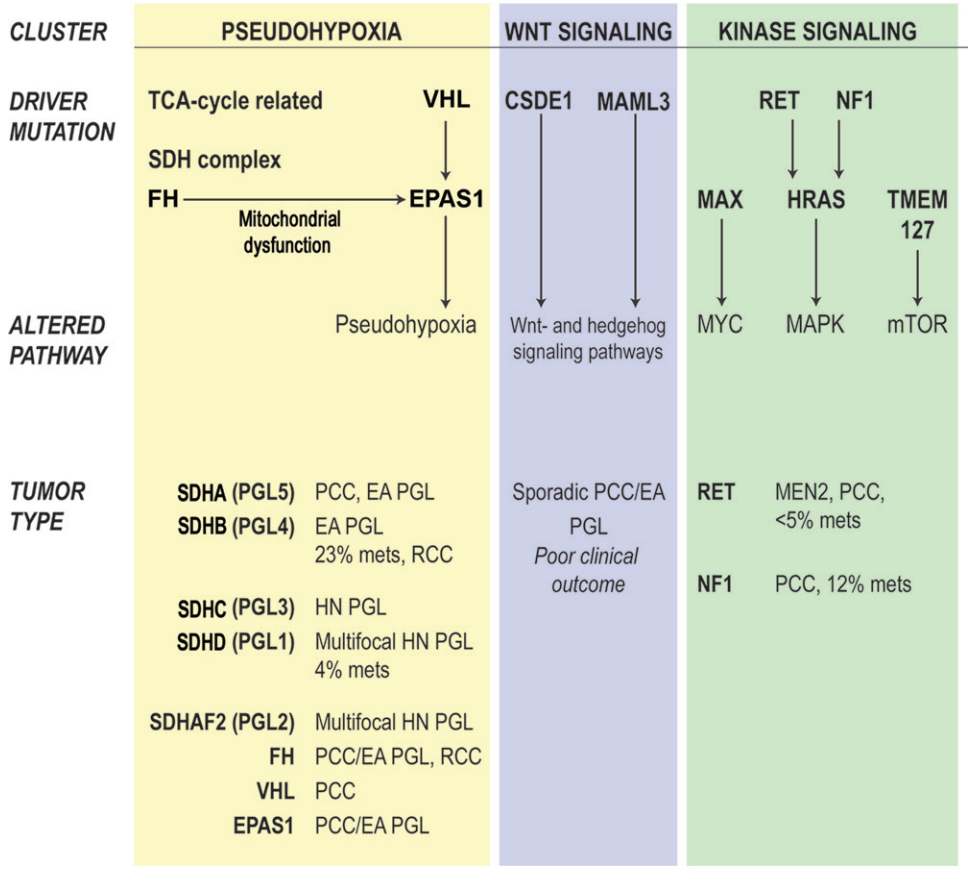


Figure 3: Summary of molecular clusters, as defined by their driver mutations, altered molecular pathways, and tumor types. *CSDE1* = cold-shock domain containing e1, EA = extra-adrenal, *EPAS1* = endothelial pas domain-containing protein 1, *FH* = fumarate hydratase, HN = head and neck, *HRAS* = HRas proto-oncogene, MAPK = mitogen-activated protein kinase, *MAX* = myc-associated factor X, *MAML3* = mastermind-like 3, MEN2 = multiple endocrine neoplasia type 2, mTOR = mammalian target of rapamycin, MYC = myc proto-oncogene, *NF1* = neurofibromatosis 1, PCC = pheochromocytoma, PGL = paraganglioma, RCC = renal cell carcinoma, *RET* = rearranged during transfection, SDH = succinate dehydrogenase, SDHAF2 = SDH complex assembly factor 2, TCA = tricarboxylic-acid, *TMEM 127* = transmembrane protein 127, *VHL* = von Hippel Lindau, Wnt = wingless and Int-1. (Reprinted, with permission, from University of Rochester, Rochester, New York © 2022; illustration by Nazdezhda D. Kiriyak.)

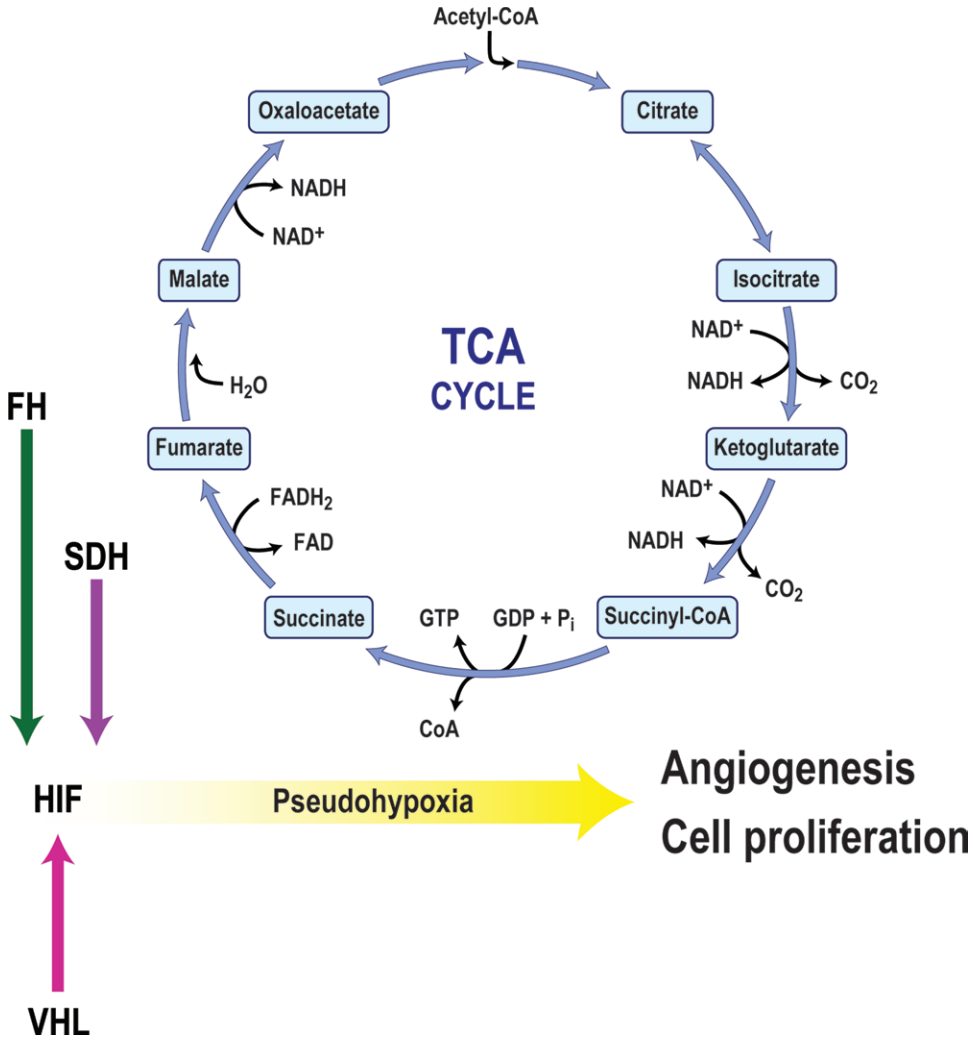


Figure 4: Relationship between tricarboxylic acid (TCA) cycle and pseudohypoxia pathways. Mutations of succinate dehydrogenase (SDH) and fumarate hydratase (FH) enzymes lead to stabilization of hypoxia inducible factor–α (HIFα), resulting in angiogenesis and cell proliferation. CoA = coenzyme A, FAD = flavin adenine dinucleotide, $FADH_2$ = 1,5-dihydro-flavin adenine dinucleotide, GDP = guanosine diphosphate, GTP = guanosine-5′-triphosphate, NAD = nicotinamide adenine dinucleotide, *VHL* = von Hippel Lindau. (Reprinted, with permission, from University of Rochester, Rochester, New York © 2022; illustration by Nazdezhda D. Kiriyak.)

This cluster includes tumors with germline pathogenic variants in several genes including von Hippel Lindau *(VHL)*, *SDHx* (group of genes giving rise to SDH complex), or fumarate hydratase, the latter two of which are involved in the mitochondrial tricarboxylic acid cycle. Some tumors in this cluster without germline pathogenic variants have somatic mutations in *VHL* and endothelial PAS domain-containing protein 1 *(EPAS1)* (encoding protein hypoxia-inducible factor [HIF] 2α) (7,28,29). Tricarboxylic acid cycle (*SDHx*/fumarate hydratase)– and *VHL*/*EPAS1*-related mutations lead to persistence of HIFα by various pathways despite the presence of normal oxygen saturation (Fig 3).

HIFα is involved in oxygen homeostasis and is typically degraded under normal oxygen saturation. When active in tumors, HIFα activates transcription of HI pathway genes and allows angiogenic tumor growth. The pseudohypoxia cluster name, therefore, denotes the effects of HI pathways under normal oxygen environments. While still being completely elucidated, pathogenic variants in *SDH* genes lead to complex II dysfunction, elevated succinate levels, inhibition of prolyl hydroxylase (which typically regulates HIFα, thereby leading to increased activity of HIFα), and inhibition of DNA demethylases, leading to global tumor DNA hypermethylation (7).

HNPGLs are predominantly associated with either sporadic disease or germline *SDHx* variants (hereditary PGL-PCC syndromes). Patients with hereditary *SDHx* pathogenic variants typically present with a mean age in the 30s, with each gene *(SDHA*, *SDHB*, *SDHC*, *SDHD*, and *SDHAF2)* having different genotype-phenotype correlations. Carriers of *SDHB* variants may have EAPGLs, PCCs, and, less commonly, HNPGLs, with approximately 23%–25% incidence of metastasis (30), the highest of all PPGL-associated genes. Carriers of *SDHD*/*SDHAF2* mutations are at highest risk for multifocal HNPGLs. *SDHD* carriers can have multifocal EAPGLs and PCCs as well, with

metastases occurring in about 8% (31). ^{68}Ga-DOTATATE, which will be discussed in detail in the section on functional imaging, demonstrates superior lesion detectability for PGLs with the *SDHB* mutation compared with other modalities. The other molecular clusters are much less frequently associated with HNPGL and will be only briefly reviewed here.

Biochemical Profiles of Specific Genetic Mutations

Gene Mutation	Molecular Cluster	Biochemical Profile
SDHx or *VHL*	Pseudohypoxia	Noradrenergic
SDHx (often *SDHB*)	Pseudohypoxia	Dopaminergic or Methoxytyramine
RET or *NF1*	Kinase-signaling	Adrenergic

Note.—*NF1* = neurofibromatosis 1, *RET* = rearranged during transfection, *SDH* = succinate dehydrogenase, *VHL* = von Hippel Lindau.

Kinase-signaling cluster.— The kinase-signaling cluster was identified early in PPGL classification (7) and confirmed in later studies (8). Tumors in this cluster are often adrenergic PCCs that can be bilateral and adrenergic PGLs, all with longer metastatic-free survival (8). In contrast to tumors in the pseudohypoxia cluster, hypermethylation is absent (8), allowing for high expression of *PNMT* and increased conversion of norepinephrine to epinephrine (32). This cluster is associated with germline pathogenic variants in *r*earranged during transfection (*RET)* and neurofibromatosis 1 genes, as well as some other more rare genes (33,34). Neurofibromatosis 1/*RET* mutations are associated with an increased activation of signaling pathways leading to cellular proliferation.

Wnt-altered cluster.— The Wnt-altered cluster was newly described in the TCGA study (8), which discovered recurrent somatic mastermind-like 3 *(MAML3)* fusion genes and cold-shock domain-containing E1 *(CSDE1)* somatic mutations. Tumors arising in this cluster have activated Wnt and sonic hedgehog signaling pathways and are strongly associated with sporadic (not inherited) PCC, depressed *PNMT* expression, and increased norepinephrine secretion. Tumors in this cluster are associated with worse clinical outcomes, metastatic disease, and higher Ki-67 indexes (8).

Biochemical and Genetic Testing

Patients with suspected PPGLs should undergo plasma-free or 24-hour urinary-fractionated metanephrine screening (sensitivities > 90% for secreting PPGLs) (4). While metanephrine screening is recommended for HNPGLs, less than 4% of HNPGLs secrete catecholamines (15). The rationale for screening patients with HNPGLs is to detect a second, potentially secreting, primary PPGL, as 50% of patients with HNPGLs will have a germline mutation in a known susceptibility gene, leading to an increased risk for multifocal disease. Although catecholamine testing is not routinely performed, given its lower specificity, it occasionally identifies PPGL in patients with *SDHx* mutations, as they may only have dopamine-secreting tumors (Table).

Guidelines recommend consideration of genetic testing in all patients with confirmed PPGLs, as 40% of patients with PPGL have germline mutations and about 25% of patients with *SDHB* mutations have metastasis (4). Hereditary syndrome diagnosis may lead to earlier detection of tumors in affected relatives (4). A large multi-institutional study revealed HNPGLs in greater than 50% of patients with *SDHx* mutations, supporting genetic testing in all patients with HNPGLs (35). Factors that increase likelihood for underlying genetic cause include early presenting age, positive family history, syndromic presentation, bilateral PCCs, multifocal PGLs, HNPGLs, and metastasis; however, even apparently sporadic tumors can have a hereditary cause (24).

Recent Advances in Imaging

CT and MRI

Imaging is performed in patients with confirmed elevated metanephrine and catecholamine secretion or suspected neck mass. Contrast-enhanced MRI is often the preferred modality used in detecting and characterizing HNPGLs, with sensitivities and specificities of 90%–95% and 92%–99%, respectively (35).

Contrast-enhanced CT also provides excellent anatomic delineation and spatial resolution and may have slightly greater sensitivity in detecting tumors smaller than 1 cm. CT is advantageous in characterizing skull base invasion and detecting small PGL tympanicum and jugulotympanicum. HNPGLs often demonstrate avid homogeneous enhancement at contrast-enhanced CT, whereas schwannomas tend to exhibit mild and inhomogeneous enhancement.

Figure 5 illustrates typical CT and MRI characteristics of common HNPGLs. The presence of intralesional hemorrhage, slow vascular flow, and vascular flow voids ("salt and pepper") are more specific for PGLs when differentiating from similar-appearing tumors such as schwannomas, meningiomas, endolymphatic sac tumor, myeloma, and metastasis. Flow voids are observed in about half of HNPGLs and are often absent in small tumors (<1 cm) (36).

Contrast-enhanced MRI combined with contrast-enhanced MR angiography (MRA) is more accurate in helping detect HNPGLs, particularly smaller tumors, compared with contrast-enhanced MRI alone, with sensitivities and specificities of 100% and 94% versus 94% and 41%, respectively (36,37). Contrast-enhanced MRA also reveals early intense arterial enhancement in HNPGLs compared with non-PGL tumors (37). The larger field of view of three-dimensional contrast-enhanced MRA relative to conventional contrast-enhanced MRI and three-dimensional time-of-flight MRA can improve detection of multifocal PGLs (37). Use of three-dimensional contrast-enhanced MRA

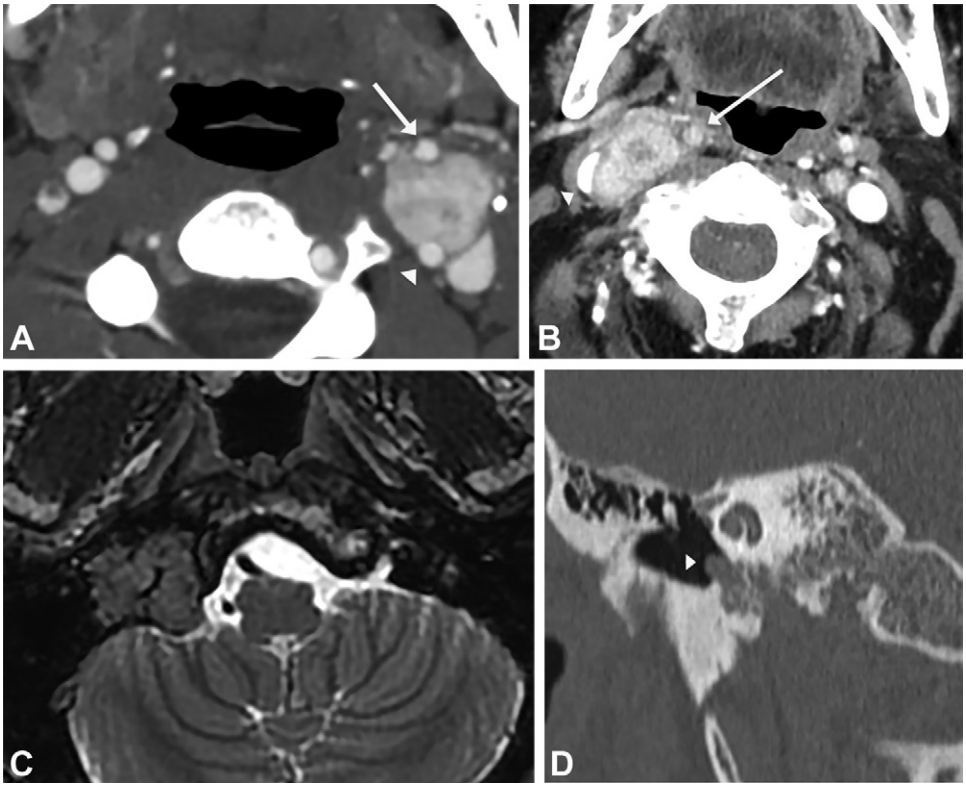


Figure 5: Typical imaging characteristics of head and neck paragangliomas. **(A)** Left carotid body paraganglioma on axial contrast-enhanced CT angiographic image, with splaying of internal carotid (arrowhead) and external carotid (arrow) arteries. **(B)** Right vagal paraganglioma on axial contrast-enhanced CT image, with anteromedial displacement of internal carotid artery (arrow) and posterolateral displacement of internal jugular vein (arrowhead). **(C)** Right jugular paraganglioma on axial T2-weighted MR image with intralesional flow voids. **(D)** Right jugulotympanic paraganglioma (arrowhead) on coronal noncontrast CT image extending into hypotympanum.

may improve diagnostic accuracy in assessing for residual or recurrent PGLs following treatment.

While conventional MRI techniques focus on anatomic, morphologic, and soft-tissue signal characteristics of PGLs, advanced MRI techniques can assess other parameters, such as blood flow and metabolite composition. MRI perfusion evaluates the delivery of blood to tissue at the capillary level over time and can be performed without contrast material by using a technique known as arterial spin labeling or with a rapid intravenous bolus of gadolinium-based contrast material using one of two techniques, dynamic susceptibility contrast MRI or dynamic contrast-enhanced (DCE) MRI. Each technique offers different strengths and disadvantages, as well as a slightly different array of perfusion parameters, which are beyond the scope of this article.

MRI perfusion may aid in differentiating HNPGLs from non-PGL tumors (38,39). Arterial spin labeling reveals markedly elevated blood flow (Fig 6) in contrast to schwannomas (38). DCE MRI helps evaluate blood flow hemodynamics by measuring the effect of intravascular contrast material as it passes through tissue over time, arriving at semiquantitative parameters such as time to peak, maximum signal difference, and signal enhancement ratio, which may further differentiate PGLs from other pathologic conditions. PGLs demonstrate a higher peak enhancement and maximum signal-enhancement ratio and shorter time to maximum enhancement compared with schwannomas (39). DCE can quantitatively evaluate how much contrast material leaks into the extravascular space from blood vessels. As PGLs contain an intense capillary network with arteriovenous shunting physiology and minimal extravascular leakage, PGLs exhibit a low K^{trans} (ie, transfer constant, measuring the combined effect of capillary permeability, blood flow, and surface area on contrast material leakage) and K_{ep} (ie, reflux rate, reflecting contrast material re-entering the blood vessel from the extravascular space) (Fig 7) (39).

MR spectroscopy uses proton nuclear MR to obtain metabolite signatures of tissue on the basis of chemical shift properties that are influenced by a compound's local atomic environment. These metabolite signatures consist of various peaks that correspond to certain compounds, such as choline, creatine, glutamate, and lactate.

Nuclear MRI is especially prone to susceptibility artifact, which is exacerbated by air and bone, making it technically challenging. While not routinely performed, MR spectroscopy demonstrates elevated succinate in *SDHx* PGLs, with a singlet peak at 2.4 ppm (Fig 7) (40,41). The succinate peak overlaps with glutamate and glutamine, though *SDHx* PGLs have been shown to have markedly depressed glutamine (40). MR spectroscopy can provide a noninvasive means of detecting *SDHx* PGLs, with a recent prospective study reporting a sensitivity of 87% and specificity of 100% (41).

Cross-sectional Imaging Recommendations

Contrast-enhanced CT is often performed as a first-line imaging modality in evaluating patients with a neck mass, as it provides excellent spatial resolution and can help detect small tumors and bony changes. Contrast-enhanced MRI can also be used as a first-line imaging modality, as it has advantages in soft-tissue characterization and functional imaging in absence of ionizing radiation. When imaging patients who present with a neck mass, adding arterial spin labeling to routine imaging may assist in identifying hypervascular masses such as PGLs and can be performed with minimal additional time. If patients are presenting with a suspected HNPGL, adding a contrast-enhanced MRA with a large field of view instead of a noncontrast MRA may offer improved detection of multifocal tumors. While DCE MRI perfusion and MR spectroscopy

can improve diagnostic accuracy and detection of PGLs, particularly with underlying *SDHx* mutation, these advanced MRI techniques require additional scanning and postprocessing time, as well as subspecialty experience.

Functional Imaging

Nuclear medicine functional imaging targets specific cell receptors to differentiate abnormal from normal tissue and to identify specific tumor cells. Fluorine 18 fluorodeoxyglucose (^{18}F-FDG), for instance, is a glucose analog that is transported via glucose transporters and accumulated in tumor cells to a much greater degree compared with normal cells, providing the contrast resolution needed to detect primary tumor and metastasis in the background of normal tissue. SSTR analogs such as DOTATATE have great affinity for subtype 2 receptors (SSTR2), which are overexpressed in EAPGLs, thus allowing for excellent detection of these tumors. Functional imaging exploits tumor-specific ligands linked to a detectable radiotracer to maximize sensitivity and specificity in lesion detectability, albeit with less anatomic resolution than CT and MRI.

Functional imaging is now indicated for initial staging or posttreatment management of PGL metastasis and may determine eligibility for systemic targeted radiation therapy. Although prospective trials comparing specific radiotracers are limited, several well-performed studies provide strong evidence to guide functional imaging recommendations. Studies have identified associations of PPGL-related genomic alterations with phenotypic cell membrane transporters and metabolic aberrations (42,43). Except for ^{18}F dihydroxyphenylalanine (DOPA) PET, these functional imaging modalities are widely available in the United States. ^{68}Ga-SSTR imaging remains expensive relative to other modalities, but costs have reduced as more studies are performed routinely.

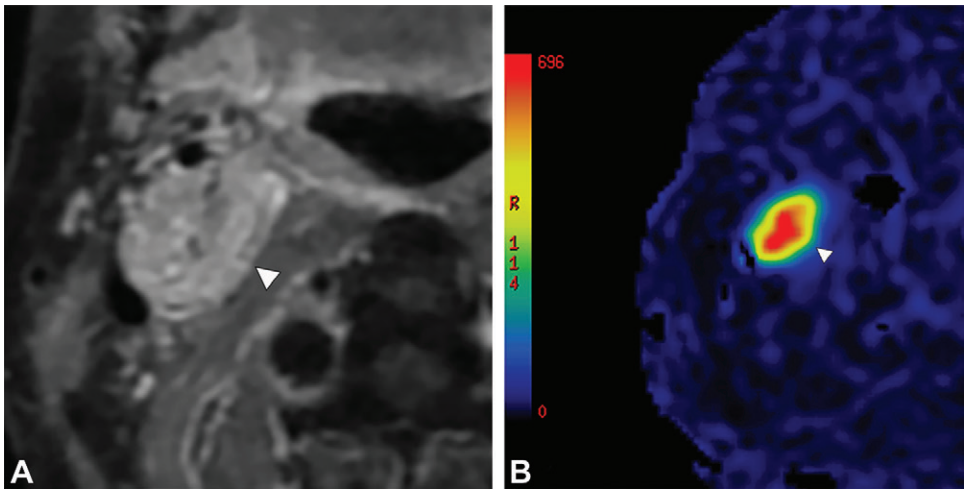


Figure 6: **(A)** Axial contrast-enhanced T1-weighted MR image demonstrates vagal paraganglioma (arrowhead) with splaying of internal carotid artery and internal jugular vein. **(B)** Corresponding increased blood flow of the vagal paraganglioma (arrowhead) on arterial spin labeling perfusion.

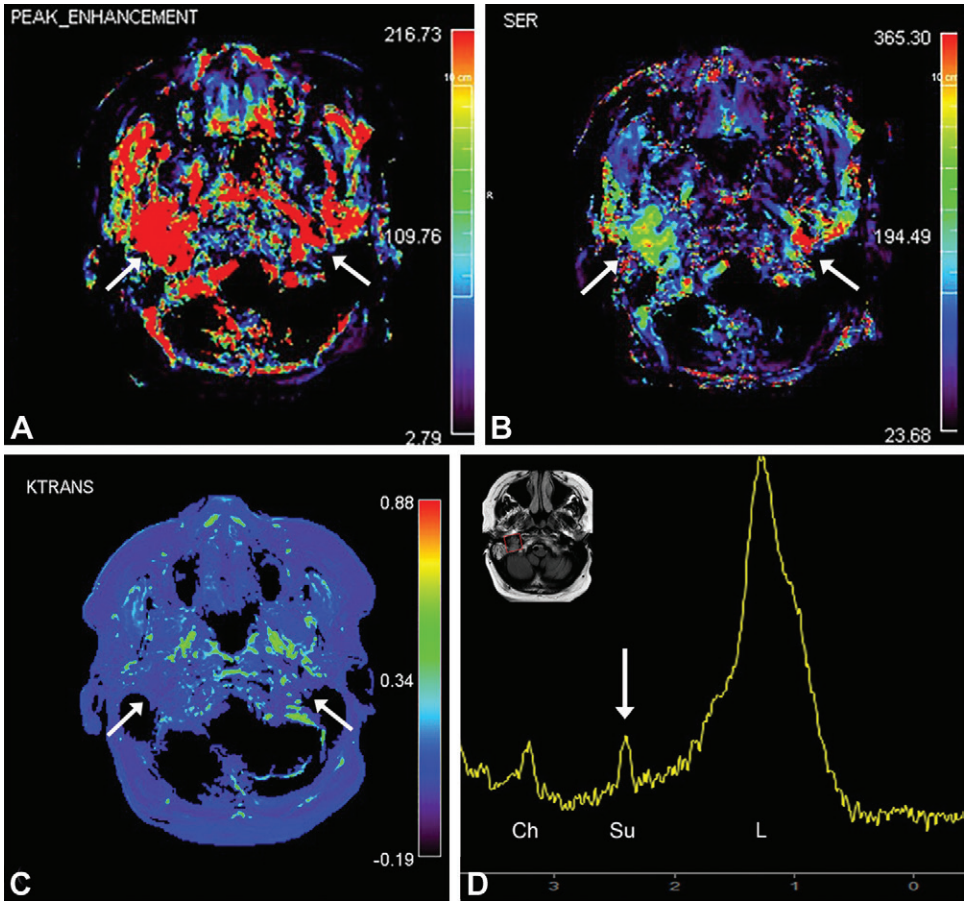


Figure 7: Axial T1-weighted dynamic contrast-enhanced perfusion MR image of bilateral jugular paragangliomas (arrows) with confirmed succinate dehydrogenase subunit B mutation, reveals **(A)** increased time to maximum enhancement, **(B)** high maximum signal-enhancement ratio (SER), and **(C)** low volume transfer constant (K^{trans}), a measure of capillary permeability. **(D)** MR spectroscopy image demonstrates elevated succinate (Su) at 2.4 ppm. Ch = choline, L = lipid or lactate.

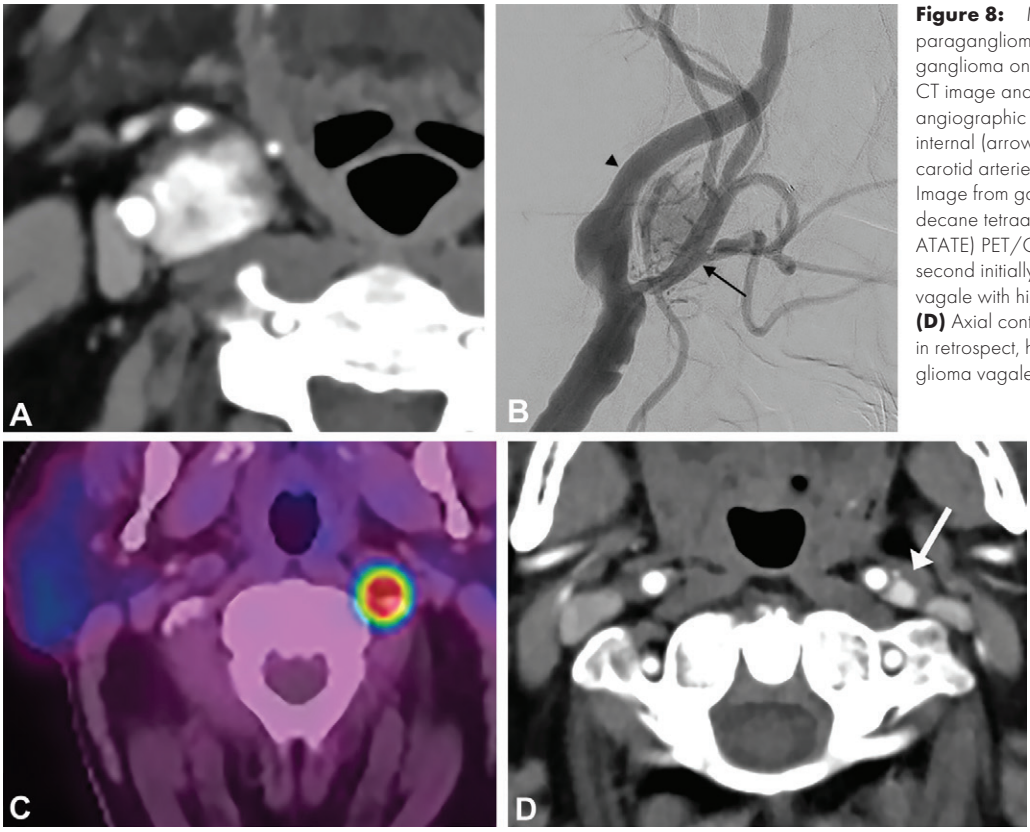


Figure 8: Multifocal head and neck paragangliomas. Right carotid body paraganglioma on **(A)** axial contrast-enhanced CT image and **(B)** digital subtraction angiographic image, with splaying of the internal (arrowhead) and external (arrow) carotid arteries in the shape of a lyre. **(C)** Image from gallium 68 tetraazacyclododecane tetraacetic acid octreotate (DOTATATE) PET/CT following resection shows second initially missed left paraganglioma vagale with high DOTATATE avidity (red). **(D)** Axial contrast-enhanced CT image, in retrospect, helps confirm left paraganglioma vagale (arrow).

^{68}Ga-SSTR imaging (^{68}Ga-DOTA-SSTR PET/CT).— ^{68}Ga, a PET radiometal, is chelated to SSTR ligands Tyr3-octreotide (DOTATOC), DOTATATE (Tyr3-octreotate), or Nal3-octreotide (or, DOTANOC). Most PPGLs highly express SSTRs (44), with ^{68}Ga-DOTATATE demonstrating extremely high subnanomolar binding affinity for SSTR2 (45). Copper 64 (^{64}Cu) DOTATATE similarly binds to SSTR2 with comparable diagnostic accuracy to ^{68}Ga DOTATATE, with improved flexibility in manufacturing and distribution due to a longer physical half-life (^{64}Cu $t_{1/2}$ = 12.7 vs ^{68}Ga $t_{1/2}$ = 1.1 hours).

^{68}Ga-SSTR agents demonstrate superior lesion detectability for EAPGLs over other functional and anatomic imaging modalities, with sensitivities approaching 100%. A systematic meta-analysis of ^{68}Ga-DOTA-SSTR revealed a pooled detection rate of 93% (^{68}Ga-DOTA-SSTR) compared with 80% (^{18}F fluoro-L-dihydroxyphenylalanine [^{18}F-DOPA] PET), 74% (^{18}F-FDG PET), and 38% (iodine 123 or 131 [^{123}I or ^{131}I] metaiodobenzylguanidine [MIBG]) (46).

^{68}Ga-DOTA-SSTR is highly accurate in detecting HNPGLs (Fig 8). ^{68}Ga-DOTATOC PET is comparable to ^{18}F-DOPA PET for nonmetastatic HNPGLs and superior to ^{18}F-DOPA PET (100% vs 56%) for metastatic HNPGLs (Fig 9), with an overall per-lesion detection rate of 100% (^{68}Ga-DOTATOC PET) compared with 71% (^{18}F-DOPA PET) (47). Subsequent prospective studies confirmed a higher detection rate of ^{68}Ga-DOTATATE over other imaging modalities, including CT and MRI, for *SDHB* PPGLs (48), *SDHD* and sporadic PPGLs (49), and HNPGLs (49–51), with rates of 94%–100%.

In detecting metastasis, ^{68}Ga-DOTATATE PET/CT demonstrated superior lesion detectability compared with CT and MRI. A prospective study evaluating HNPGLs revealed significantly higher lesion detectability ($P < .01$) of ^{68}Ga-DOTATATE PET/CT (100%, 38 of 38) over CT and MRI (61%, 23 of 38) (50). For sporadic metastatic PPGL, ^{68}Ga-DOTATATE PET/CT lesion detectability of 98% (450 of 461) was significantly higher than CT and MRI (82%, 376 of 461) ($P < .01$) (48). For *SDHB* PPGLs, ^{68}Ga-DOTATATE PET/CT lesion detectability of 99% was significantly higher ($P < .01$) than CT and MRI detectability (85%) (48).

Not much is known about HNPGLs with low or decreased SSTR expression where ^{68}Ga-DOTATATE may not be useful. False-negative ^{68}Ga-DOTATATE results are typically reported for PPGLs without specific reference to HNPGLs. Although PPGLs with associated polycythemia syndrome have reported a relatively low ^{68}Ga-DOTATATE sensitivity (35%), none of the 14 participants in this study contained HNPGLs (52). As neuroendocrine tumors dedifferentiate, loss of SSTR cell surface marker expression may occur, resulting in low ^{68}Ga-DOTATATE uptake. In these cases, however, an aggressive phenotype may be detected by FDG PET/CT.

The current National Comprehensive Cancer Network guidelines 1.2019 (March 2019) for evaluation of PPGL are broadly written and recommend functional evaluation for suspected metastasis with MIBG, SSTR-based imaging, FDG PET/CT, or bone scan (if bone symptoms exist). The updated European Association of Nuclear Medicine/Society of Nuclear Medicine practice guidelines are more specific

and recommend ^{68}Ga-DOTATATE PET as first-line imaging for HNPGLs, with F-DOPA and FDG PET/CT (or indium 111 [^{111}In] SSTR) as second- and third-line imaging modalities, respectively (53,54). The recent North American Neuroendocrine Tumor Society guidelines on management of metastatic PPGL recommend SSTR-based imaging as first-line functional imaging in those with metastatic PPGL, especially bony metastases, with FDG PET/CT as second line. The North American Neuroendocrine Tumor Society guidelines do not recommend ^{111}In-SSTR, given the poor sensitivity (55). With current evidence, ^{68}Ga-DOTATATE PET should be recommended as first-line imaging for HNPGLs when suspecting metastases or multifocal disease and when identifying candidates for targeted peptide-receptor therapy.

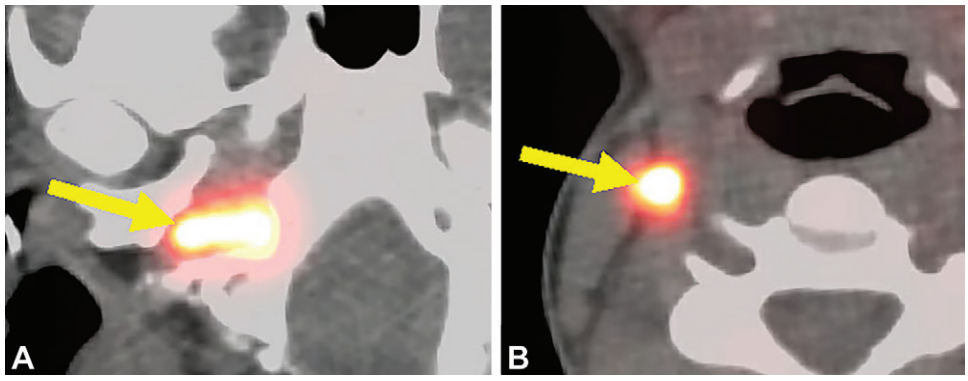


Figure 9: History of head and neck paraganglioma status after resection and radiation with succinate dehydrogenase subunit D *(SDHD)* variant. Gallium 68 tetraazacyclododecane tetraacetic acid–octreotate (ie, DOTATATE) PET/CT images show **(A)** residual skull base paraganglioma (arrow) and **(B)** metastatic right level IIb lymph node (arrow).

^{111}In-pentetreotide SPECT/CT.— ^{111}In-pentetreotide, an SSTR-ligand, has high affinity for SSTR2, but lower relative to ^{68}Ga-DOTATATE (45). Prior to Food and Drug Administration (FDA) approval of ^{68}Ga-DOTATATE, ^{111}In-pentetreotide demonstrated improved sensitivities of greater than 90% over ^{123}I-MIBG in helping detect HNPGLs (56). ^{111}In-pentetreotide has significantly lower lesion detectability of neuroendocrine tumors compared with ^{68}Ga-DOTATATE (57). Contributing factors include higher spatial resolution of PET over SPECT and greater ^{68}Ga-DOTATATE tumor uptake facilitated by higher receptor affinity (45,50). ^{111}In-pentetreotide may be useful for HNPGLs when ^{68}Ga-DOTATATE PET/CT is unavailable but is otherwise not recommended given the low sensitivity.

^{123}I and ^{131}I-MIBG SPECT/CT.— ^{123}I-MIBG, a guanethidine analog, has binding properties like noradrenalin, with high affinity for norepinephrine transporter-1, which resides on neuron cell surfaces and intracellular vesicles involved in catecholamine storage. ^{123}I-MIBG exhibits a high target-to-background ratio that is favorable for imaging.

MIBG has high sensitivity (85%–98%) and specificity (>90%) for primary PPGLs, with higher detection of PCCs than EAPGLs (58). MIBG remains inferior to SSTR-based imaging, particularly for EAPGLs (39% vs 98% sensitivity) and HNPGLs (22% vs 100% sensitivity) (59). ^{123}I-MIBG should be used primarily in identifying candidates for systemic ^{131}I-MIBG therapy (55).

^{18}F-FDG PET/CT.— ^{18}F-FDG is transported into cells and trapped intracellularly, providing a high-contrast, integrated PET signal of glycolytic activity. ^{18}F-FDG PET/CT has higher sensitivity in helping detect nonmetastatic and metastatic HNPGLs relative to MIBG (83% vs 50%) (60). Metastatic lesions frequently exhibit greater FDG avidity relative to primary tumor, making ^{18}F-FDG PET/CT a good alternative for assessing metastatic burden (61,62). ^{18}F-FDG PET/CT is recommended as alternative functional imaging for HNPGLs and metastasis if ^{68}Ga DOTATATE is not available (43,54).

^{18}F-DOPA PET/CT.— Decarboxylate amino acid analogs, such as F-DOPA, are taken up by neutral amino acid system L-amino transporters commonly expressed on PPGLs. Many studies revealed less than 90% sensitivities in detecting PGLs by using ^{18}F-DOPA (49,61,63). Prior to ^{68}Ga DOTATATE, F-DOPA was considered an excellent radiotracer for functional imaging of PGLs. Subsequent studies confirmed superiority of ^{68}Ga-DOTATATE over F-DOPA, particularly for metastasis. F-DOPA is primarily available in Europe, with limited availability in the United States.

^{18}F-Fluorodopamine PET/CT.— In ^{18}F-fluorodopamine, F-dopamine is taken up by neuroendocrine cells via norepinephrine transporter, demonstrating high diagnostic accuracy for sympathetic, but not for parasympathetic, PGLs. In a prospective study of 20 participants with known HNPGL, ^{68}Ga DOTATATE demonstrated the highest detectability of head and neck lesions of 100% (38 of 38) and of metastatic lesions outside of the head and neck of 100% (30 of 30). In patients who also underwent ^{18}F-fluorodopamine PET/CT (18 of 20), detectability was 29% (10 of 34) for head and neck lesions and 30% (eight of 27) for lesions outside of the head and neck (50).

Functional Imaging Recommendations

While CT and MRI are typically performed as first-line imaging for patients presenting with a neck mass or suspected HNPGL, ^{68}Ga-DOTATATE PET, when available, should be used as first-line imaging for patients with a known HNPGL, particularly with underlying *SDHx* mutation, and known or potential metastatic and/or multifocal disease. ^{68}Ga-DOTATATE PET can also be performed when identifying candidates for targeted peptide-receptor therapy. When ^{68}Ga-DOT-

ATATE PET is not an option, potential alternatives include ^{111}In-pentetreotide for primary HNPGLs and ^{18}F-FDG PET/CT for evaluation of metastasis, especially in HNPGLs with low SSTR expression. ^{123}I-MIBG should be used primarily in identifying candidates for ^{131}I-MIBG therapy.

Treatment

HNPGLs exhibit variable growth characteristics but are typically slow-growing tumors, with approximately 40% in one study demonstrating less than 20% growth over a mean 4-year follow-up time (64). Initial observation is a reasonable option for patients with smaller (<2–3 cm) asymptomatic and nonfunctional HNPGLs (15).

HNPGLs have historically been treated with surgical resection, which, in general, is still recommended as definitive treatment for larger (>2–3 cm), rapidly enlarging, functional, and/or symptomatic tumors, particularly carotid body and vagal PGLs. Presurgical biopsy is contraindicated in patients with catecholamine-secreting PGLs. Cure rates of greater than 90% have been achieved following gross total resection of nonmetastatic carotid body and vagal PGLs (65–67). Surgical resection via tympanoplasty is also the treatment of choice for symptomatic tympanic PGLs, as these often manifest at an earlier stage (68). Optimal treatment of jugular and jugulotympanic PGLs is more controversial and is dependent on the patient's overall health, symptoms, preference, and size and extent of the tumor, with some patients with skull base PGLs opting for radiation therapy given the complexity of surgery and potential for cranial nerve complications.

Preoperative medical blockade, such as with α-adrenergic receptor blockers, is indicated in all patients with secreting tumors, though the majority of HNPGLs are nonfunctional. Secreting PPGLs in patients with multifocal PPGLs should be treated and resected prior to resection of nonsecreting HNPGLs. Carotid body and vagal PGLs are typically resected using a transcervical approach. Cranial nerve injury remains the greatest complication risk of surgery, followed by bleeding and stroke (69).

Prior to resecting HNPGLs, some patients may undergo perioperative embolization to reduce intraoperative bleeding. While no consensus on preoperative embolization exists, a meta-analysis concluded that embolization overall reduced blood loss and operative time (70). While embolization carries a risk for stroke, vascular dissection, and cranial nerve palsies, intraoperative risk of carotid artery injury increases with greater contact between the tumor and artery, particularly Shamblin group III carotid body PGLs. The overall benefits of preoperative embolization should outweigh the potential risks.

Radiation therapy is a reasonable alternative for nonsurgical candidates, tumors in surgically challenging anatomic locations that may portend a high risk for cranial nerve or vascular injury or sacrifice, tumor control following subtotal resection, local recurrence, and patients with pre-existing contralateral vagal nerve palsy. Radiation therapy can be delivered using conventionally fractionated external beam radiation (45–50 Gy in doses of approximately 2 Gy per day) or single-fraction (12–15 Gy) or hypofractionated (12–15 Gy over several days) stereotactic radiosurgery. HNPGLs treated with radiation therapy may slightly decrease in size but will not significantly decrease in overall volume. Radiation therapy is, therefore, not recommended as curative treatment for large, functional, and/or symptomatic tumors that may be potentially treated by surgery, as radiation therapy may not alleviate symptoms or compression of neurovascular structures. Tumor control rates are generally around 90% or greater for carotid body, vagal, and jugulotympanic PGLs (66,67,71,72).

Acute and long-term sequelae of radiation therapy have been reported in the treatment of HNPGLs, including skin erythema, mucositis, and xerostomia, as well as hearing loss and cranial nerve deficits, which occur less commonly after radiation therapy than they do after surgery. Skull base osteomyelitis and necrosis and brain necrosis can still occur but are much less common with the advent of conformal radiation therapy.

Optimal treatment for locally advanced skull base PGLs, such as jugular and jugulotympanic PGLs, remains controversial. Surgical resection is technically challenging, with a considerable risk for neurovascular injury. While radiation therapy may not alleviate symptoms related to size and compression of neurovascular structures, it is associated with less risk for cranial nerve palsies and may offer greater benefit relative to risk for advanced nonfunctional skull base PGLs (66,67).

Chemotherapy with cyclophosphamide, vincristine, and dacarbazine has been offered to patients with metastasis, though no prospective randomized clinical trials have been performed to confirm efficacy, and overall response rates are low. Complete or partial tumor response has been reported as between 4% and 37% (73). Chemotherapy or targeted agents can be considered in patients with unresectable, rapidly progressive PGLs with extensive metastasis, particularly bone metastasis. Genetic data may influence future therapies, as PPGLs with germline *SDHB* mutations may respond better to cyclophosphamide, vincristine, and dacarbazine than those with sporadic disease (74). *SDHB*-related PPGLs are associated with DNA hypermethylation and may respond well to temozolamide (75), which has been used in patients with glioma with hypermethylated *MGMT*. Radiation therapy for metastasis has been controversial and can be used for local tumor control, symptomatic relief, and painful bony metastasis, though recent studies demonstrated tumor control in 87% of patients with metastasis (76,77). Theranostic agents can also be used to treat metastatic PPGLs, discussed further below.

Theranostics

Theranostics refers to therapeutic nuclear medicine, using peptide receptor–mediated radionuclides to target specific pathologic tissue and deliver therapeutic radiation doses. The therapeutic effect is determined by multiple factors, including stability, pharmacokinetics, tissue distribution and affinity of the radionuclide, and radiosensitivity of the target cells. Diagnostic radionuclides can predetermine the potential therapeutic effect of a theranostic agent. For example, tumor avidity of ^{123}I-MIBG by using norepinephrine transporter may help predict ^{131}I-MIBG uptake. A recent prospective trial with ^{131}I-MIBG showed 92% partial response or stable disease within 12

months for advanced PPGLs (78), leading to FDA approval of the only radionuclide therapy for MIBG scan–positive, unresectable, locally advanced or metastatic PPGL.

Current studies are evaluating outcomes of ^{68}Ga-DOTATATE–positive PPGL treated with lutetium 177 (^{177}Lu) DOTA-octreotate. In patients with gastroenteropancreatic neuroendocrine tumors and positive SSTR imaging, ^{177}Lu-DOTA-octreotate significantly improved progression-free survival (79), leading to its FDA approval. In a case series, ^{177}Lu-DOTATATE demonstrated 85% partial response or stable disease in patients with progressive metastatic PPGLs (80). A meta-analysis of SSTR-ligand radiation therapy of PPGL patients revealed 25% response rate and 84% disease control (81). These efficacy data support ^{177}Lu-DOTATATE as a novel therapeutic option for patients with SSTR imaging–positive PPGL with locally unresectable or metastatic disease. Prospective clinical trials are ongoing.

Posttreatment Surveillance

While the risk of local recurrence in patients who have undergone gross total resection of nonmetastatic HNPGLs is low, continued clinical, laboratory, and imaging surveillance is recommended for all patients following definitive treatment. Local recurrence, metachronous lesions, and distant metastasis may occur at any time, including many years following primary treatment. Cross-sectional imaging should be performed within 4–6 months following gross total resection and perhaps earlier in patients following subtotal resection. In patients with sporadic disease (no known germline predisposition), annual routine surveillance can be continued for 3 years in patients without local recurrence or with stable disease. The interval of surveillance can be lengthened thereafter, such as to every other year for 6 years and every 3 years for the remainder, although no formal guidelines exist on this. Patients with a higher risk for multifocal and metastatic disease, such as those with known genetic alterations associated with PPGLs, should undergo closer interval follow-up, such as with annual screening. Depending on altered susceptibility gene, different guidelines for screening and surveillance exist (82,83). Local recurrence and metachronous lesions should be treated promptly.

Conclusion

PPGLs are neuroendocrine tumors that derive from paraganglia associated with the autonomic system and are often genetically driven. Germline pathogenic variants in known susceptibility genes have been identified in 40% of all PPGLs, several of which are associated with an increased risk for multifocal *(SDHD)* and metastatic (*SDHB)* disease. An evolving molecular classification has uncovered at least three molecular clusters—pseudohypoxia, kinase-signaling, and Wnt-altered—which may have prognostic indications. HNPGLs, which derive from parasympathetic paraganglia and are predominantly nonfunctional, are largely related to pseudohypoxia and have been previously excluded from most molecular profiling studies, which is an area of future research. Genetic testing is recommended for all patients with PPGLs to guide screening and surveillance for patients and close relatives. Advanced MRI techniques, such as MR perfusion and MR spectroscopy, may improve sensitivity and specificity but are technically challenging to perform. ^{68}Ga-DOTATATE PET is recommended as first-line imaging in patients with a known HNPGL and metastatic disease, or when at high risk for metastasis and/or multifocal disease. Surgical resection is still recommended as definitive treatment in patients with large, rapidly progressive and/or functional cervical PGLs in the lower areas of the neck, with observation and radiation therapy as reasonable alternatives in select patients. Treatment of metastatic disease remains focused on local tumor control, symptomatic relief, and palliative care. Future studies may further elucidate the molecular basis of HNPGLs and the efficacy and role of theranostics in the treatment of patients with unresectable or metastatic disease.

Disclosures of conflicts of interest: E.P.L. No relevant relationships. **B.B.C.** No relevant relationships. **L.F.** Some salary support from grants from National Institutes of Health/National Cancer Institute (no. R01 CA246586-01A1) and American Cancer Society (no. MRSG-15-063-01-TBG); consultant to Azedra executive advisory panel, no payments so far but there may be in the future; leadership or fiduciary role as clinical science chair for Endocrine Society Annual Meeting Steering Committee (unpaid), chair for Neuroendocrine Tumor Society Guidelines Committee (unpaid), and PheoPara Alliance Medical advisory board member (unpaid). **T.M.** No relevant relationships. **S.P.M.** No relevant relationships. **S.E.** No relevant relationships. **S.N.** No relevant relationships.

References

1. Beard CM, Sheps SG, Kurland LT, Carney JA, Lie JT. Occurrence of pheochromocytoma in Rochester, Minnesota, 1950 through 1979. Mayo Clin Proc 1983;58(12):802–804.
2. Stenström G, Svärdsudd K. Pheochromocytoma in Sweden 1958-1981. An analysis of the National Cancer Registry Data. Acta Med Scand 1986;220(3):225–232.
3. Favier J, Amar L, Gimenez-Roqueplo AP. Paraganglioma and phaeochromocytoma: from genetics to personalized medicine. Nat Rev Endocrinol 2015;11(2):101–111.
4. Lenders JW, Duh QY, Eisenhofer G, et al. Pheochromocytoma and paraganglioma: an endocrine society clinical practice guideline. J Clin Endocrinol Metab 2014;99(6):1915–1942.
5. Castro-Vega LJ, Lepoutre-Lussey C, Gimenez-Roqueplo AP, Favier J. Rethinking pheochromocytomas and paragangliomas from a genomic perspective. Oncogene 2016;35(9):1080–1089.
6. Hescot S, Leboulleux S, Amar L, et al. One-year progression-free survival of therapy-naive patients with malignant pheochromocytoma and paraganglioma. J Clin Endocrinol Metab 2013;98(10):4006–4012.
7. Dahia PL, Ross KN, Wright ME, et al. A HIF1alpha regulatory loop links hypoxia and mitochondrial signals in pheochromocytomas. PLoS Genet 2005;1(1):72–80.
8. Fishbein L, Leshchiner I, Walter V, et al. Comprehensive molecular characterization of pheochromocytoma and paraganglioma. Cancer Cell 2017;31(2):181–193.
9. Mulligan RM. Chemodectoma in the dog. Am J Pathol 1950;26(4):680–681.
10. Dahia PL. Pheochromocytoma and paraganglioma pathogenesis: learning from genetic heterogeneity. Nat Rev Cancer 2014;14(2):108–119.
11. Burnichon N, Rohmer V, Amar L, et al. The succinate dehydrogenase genetic testing in a large prospective series of patients with paragangliomas. J Clin Endocrinol Metab 2009;94(8):2817–2827.
12. Neumann HP, Bausch B, McWhinney SR, et al. Germ-line mutations in nonsyndromic pheochromocytoma. N Engl J Med 2002;346(19):1459–1466.
13. Bausch B, Wellner U, Bausch D, et al. Long-term prognosis of patients with pediatric pheochromocytoma. Endocr Relat Cancer 2013;21(1):17–25.
14. Mannelli M, Castellano M, Schiavi F, et al. Clinically guided genetic screening in a large cohort of italian patients with pheochromocytomas and/or functional or nonfunctional paragangliomas. J Clin Endocrinol Metab 2009;94(5):1541–1547.
15. Smith JD, Harvey RN, Darr OA, et al. Head and neck paragangliomas: A two-decade institutional experience and algorithm for management. Laryngoscope Investig Otolaryngol 2017;2(6):380–389.
16. Pellitteri PK, Rinaldo A, Myssiorek D, et al. Paragangliomas of the head and neck. Oral Oncol 2004;40(6):563–575.

17. Shamblin WR, ReMine WH, Sheps SG, Harrison EG Jr. Carotid body tumor (chemodectoma). Clinicopathologic analysis of ninety cases. Am J Surg 1971;122(6):732–739.
18. Arya S, Rao V, Juvekar S, Dcruz AK. Carotid body tumors: objective criteria to predict the Shamblin group on MR imaging. AJNR Am J Neuroradiol 2008;29(7):1349–1354.
19. Netterville JL, Jackson CG, Miller FR, Wanamaker JR, Glasscock ME. Vagal paraganglioma: a review of 46 patients treated during a 20-year period. Arch Otolaryngol Head Neck Surg 1998;124(10):1133–1140.
20. Williams MD. Paragangliomas of the head and neck: an overview from diagnosis to genetics. Head Neck Pathol 2017;11(3):278–287.
21. Lloyd R, Osamura RY, Klöppel G, Rosai J. WHO classification of tumours: pathology and genetics of tumours of endocrine organs. 4th ed. Lyon, France: IARC, 2017.
22. Amin MB, Edge SB, Greene FL, et al. AJCC Cancer Staging Manual. 8th ed. New York, NY: Springer, 2017.
23. Ayala-Ramirez M, Feng L, Johnson MM, et al. Clinical risk factors for malignancy and overall survival in patients with pheochromocytomas and sympathetic paragangliomas: primary tumor size and primary tumor location as prognostic indicators. J Clin Endocrinol Metab 2011;96(3):717–725.
24. Fishbein L, Merrill S, Fraker DL, Cohen DL, Nathanson KL. Inherited mutations in pheochromocytoma and paraganglioma: why all patients should be offered genetic testing. Ann Surg Oncol 2013;20(5):1444–1450.
25. Gupta G, Pacak K; AACE Adrenal Scientific Committee. Precision medicine: an update on genotype/biochemical phenotype relationships in pheochromocytoma/paraganglioma patients. Endocr Pract 2017;23(6):690–704.
26. Letouzé E, Martinelli C, Loriot C, et al. SDH mutations establish a hypermethylator phenotype in paraganglioma. Cancer Cell 2013;23(6):739–752.
27. Tevosian SG, Ghayee HK. Pheochromocytoma/paraganglioma: a poster child for cancer metabolism. J Clin Endocrinol Metab 2018;103(5):1779–1789.
28. Burnichon N, Buffet A, Parfait B, et al. Somatic NF1 inactivation is a frequent event in sporadic pheochromocytoma. Hum Mol Genet 2012;21(26):5397–5405.
29. Welander J, Andreasson A, Brauckhoff M, et al. Frequent EPAS1/HIF2α exons 9 and 12 mutations in non-familial pheochromocytoma. Endocr Relat Cancer 2014;21(3):495–504.
30. Andrews KA, Ascher DB, Pires DEV, et al. Tumour risks and genotype-phenotype correlations associated with germline variants in succinate dehydrogenase subunit genes *SDHB*, *SDHC* and *SDHD*. J Med Genet 2018;55(6):384–394 [Published correction appears in J Med Genet 2019;56(1):50-52.].
31. van Hulsteijn LT, Dekkers OM, Hes FJ, Smit JW, Corssmit EP. Risk of malignant paraganglioma in SDHB-mutation and SDHD-mutation carriers: a systematic review and meta-analysis. J Med Genet 2012;49(12):768–776.
32. Eisenhofer G, Lenders JW, Timmers H, et al. Measurements of plasma methoxytyramine, normetanephrine, and metanephrine as discriminators of different hereditary forms of pheochromocytoma. Clin Chem 2011;57(3):411–420.
33. Burnichon N, Vescovo L, Amar L, et al. Integrative genomic analysis reveals somatic mutations in pheochromocytoma and paraganglioma. Hum Mol Genet 2011;20(20):3974–3985.
34. Castro-Vega LJ, Letouzé E, Burnichon N, et al. Multi-omics analysis defines core genomic alterations in pheochromocytomas and paragangliomas. Nat Commun 2015;6(1):6044.
35. Gimenez-Roqueplo AP, Caumont-Prim A, Houzard C, et al. Imaging work-up for screening of paraganglioma and pheochromocytoma in SDHx mutation carriers: a multicenter prospective study from the PGL. EVA Investigators. J Clin Endocrinol Metab 2013;98(1):E162–E173.
36. van den Berg R, Verbist BM, Mertens BJ, van der Mey AG, van Buchem MA. Head and neck paragangliomas: improved tumor detection using contrast-enhanced 3D time-of-flight MR angiography as compared with fat-suppressed MR imaging techniques. AJNR Am J Neuroradiol 2004;25(5):863–870.
37. Neves F, Huwart L, Jourdan G, et al. Head and neck paragangliomas: value of contrast-enhanced 3D MR angiography. AJNR Am J Neuroradiol 2008;29(5):883–889.
38. Geerts B, Leclercq D, Tezenas du Montcel S, et al. Characterization of Skull Base Lesions Using Pseudo-Continuous Arterial Spin Labeling. Clin Neuroradiol 2019;29(1):75–86.
39. Gaddikeri S, Hippe DS, Anzai Y. Dynamic Contrast-Enhanced MRI in the Evaluation of Carotid Space Paraganglioma versus Schwannoma. J Neuroimaging 2016;26(6):618–625.
40. Varoquaux A, le Fur Y, Imperiale A, et al. Magnetic resonance spectroscopy of paragangliomas: new insights into in vivo metabolomics. Endocr Relat Cancer 2015;22(4):M1–M8.
41. Lussey-Lepoutre C, Bellucci A, Burnichon N, et al. Succinate detection using in vivo ^{1}H-MR spectroscopy identifies germline and somatic SDHx mutations in paragangliomas. Eur J Nucl Med Mol Imaging 2020;47(6):1510–1517.
42. Antonio K, Valdez MMN, Mercado-Asis L, Taïeb D, Pacak K. Pheochromocytoma/paraganglioma: recent updates in genetics, biochemistry, immunohistochemistry, metabolomics, imaging and therapeutic options. Gland Surg 2020;9(1):105–123.
43. Taïeb D, Jha A, Treglia G, Pacak K. Molecular imaging and radionuclide therapy of pheochromocytoma and paraganglioma in the era of genomic characterization of disease subgroups. Endocr Relat Cancer 2019;26(11):R627–R652.
44. Reubi JC, Waser B, Khosla S, et al. In vitro and in vivo detection of somatostatin receptors in pheochromocytomas and paragangliomas. J Clin Endocrinol Metab 1992;74(5):1082–1089.
45. Reubi JC, Schär JC, Waser B, et al. Affinity profiles for human somatostatin receptor subtypes SST1-SST5 of somatostatin radiotracers selected for scintigraphic and radiotherapeutic use. Eur J Nucl Med 2000;27(3):273–282.
46. Han S, Suh CH, Woo S, Kim YJ, Lee JJ. Performance of ^{68}Ga-DOTA-conjugated somatostatin receptor-targeting peptide PET in detection of pheochromocytoma and paraganglioma: a systematic review and meta-analysis. J Nucl Med 2019;60(3):369–376.
47. Kroiss A, Putzer D, Frech A, et al. A retrospective comparison between 68Ga-DOTA-TOC PET/CT and 18F-DOPA PET/CT in patients with extra-adrenal paraganglioma. Eur J Nucl Med Mol Imaging 2013;40(12):1800–1808.
48. Janssen I, Blanchet EM, Adams K, et al. Superiority of [68Ga]-DOTATATE PET/CT to other functional imaging modalities in the localization of SDHB-associated metastatic pheochromocytoma and paraganglioma. Clin Cancer Res 2015;21(17):3888–3895.
49. Archier A, Varoquaux A, Garrigue P, et al. Prospective comparison of (68) Ga-DOTATATE and (18)F-FDOPA PET/CT in patients with various pheochromocytomas and paragangliomas with emphasis on sporadic cases. Eur J Nucl Med Mol Imaging 2016;43(7):1248–1257.
50. Janssen I, Chen CC, Taieb D, et al. 68Ga-DOTATATE PET/CT in the localization of head and neck paragangliomas compared with other functional imaging modalities and CT/MRI. J Nucl Med 2016;57(2):186–191.
51. Sharma P, Thakar A, Suman K C S, et al. 68Ga-DOTANOC PET/CT for baseline evaluation of patients with head and neck paraganglioma. J Nucl Med 2013;54(6):841–847.
52. Janssen I, Chen CC, Zhuang Z, et al. Functional imaging signature of patients presenting with polycythemia/paraganglioma syndromes. J Nucl Med 2017;58(8):1236–1242.
53. Taïeb D, Hicks RJ, Hindié E, et al. European Association of Nuclear Medicine Practice Guideline/Society of Nuclear Medicine and Molecular Imaging Procedure Standard 2019 for radionuclide imaging of phaeochromocytoma and paraganglioma. Eur J Nucl Med Mol Imaging 2019;46(10):2112–2137.
54. Bozkurt MF, Virgolini I, Balogova S, et al. Guideline for PET/CT imaging of neuroendocrine neoplasms with ^{68}Ga-DOTA-conjugated somatostatin receptor targeting peptides and ^{18}F-DOPA. Eur J Nucl Med Mol Imaging 2017;44(9):1588–1601 [Published correction appears in Eur J Nucl Med Mol Imaging 2017;44(12):2150–2151.].
55. Fishbein L, Del Rivero J, Else T, et al. The North American Neuroendocrine Tumor Society Consensus Guidelines for Surveillance and Management of Metastatic and/or Unresectable Pheochromocytoma and Paraganglioma. Pancreas 2021;50(4):469–493.
56. Koopmans KP, Jager PL, Kema IP, Kerstens MN, Albers F, Dullaart RP. 111In-octreotide is superior to 123I-metaiodobenzylguanidine for scintigraphic detection of head and neck paragangliomas. J Nucl Med 2008;49(8):1232–1237.
57. Sadowski SM, Neychev V, Millo C, et al. Prospective study of 68Ga-DOTATATE positron emission tomography/computed tomography for detecting gastro-entero-pancreatic neuroendocrine tumors and unknown primary sites. J Clin Oncol 2016;34(6):588–596.
58. Ezzat Abdel-Aziz T, Prete F, Conway G, et al. Phaeochromocytomas and paragangliomas: A difference in disease behaviour and clinical outcomes. J Surg Oncol 2015;112(5):486–491.
59. Arora S, Kumar R, Passah A, et al. Prospective evaluation of 68Ga-DOTANOC positron emission tomography/computed tomography and 131I-meta-iodobenzylguanidine single-photon emission computed tomography/computed tomography in extra-adrenal paragangliomas, including uncommon primary sites and to define their diagnostic roles in current scenario. Nucl Med Commun 2019;40(12):1230–1242.
60. Timmers HJ, Chen CC, Carrasquillo JA, et al. Staging and functional characterization of pheochromocytoma and paraganglioma by 18F-

fluorodeoxyglucose (18F-FDG) positron emission tomography. J Natl Cancer Inst 2012;104(9):700–708.
61. Timmers HJ, Chen CC, Carrasquillo JA, et al. Comparison of 18F-fluoro-L-DOPA, 18F-fluoro-deoxyglucose, and 18F-fluorodopamine PET and 123I-MIBG scintigraphy in the localization of pheochromocytoma and paraganglioma. J Clin Endocrinol Metab 2009;94(12):4757–4767.
62. Taïeb D, Timmers HJ, Shulkin BL, Pacak K. Renaissance of (18)F-FDG positron emission tomography in the imaging of pheochromocytoma/paraganglioma. J Clin Endocrinol Metab 2014;99(7):2337–2339.
63. King KS, Chen CC, Alexopoulos DK, et al. Functional imaging of SDHx-related head and neck paragangliomas: comparison of 18F-fluorodihydroxyphenylalanine, 18F-fluorodopamine, 18F-fluoro-2-deoxy-D-glucose PET, 123I-metaiodobenzylguanidine scintigraphy, and 111In-pentetreotide scintigraphy. J Clin Endocrinol Metab 2011;96(9):2779–2785.
64. Jansen JC, van den Berg R, Kuiper A, van der Mey AG, Zwinderman AH, Cornelisse CJ. Estimation of growth rate in patients with head and neck paragangliomas influences the treatment proposal. Cancer 2000;88(12):2811–2816.
65. Papaspyrou K, Mann WJ, Amedee RG. Management of head and neck paragangliomas: review of 120 patients. Head Neck 2009;31(3):381–387.
66. Suárez C, Rodrigo JP, Bödeker CC, et al. Jugular and vagal paragangliomas: Systematic study of management with surgery and radiotherapy. Head Neck 2013;35(8):1195–1204.
67. Hinerman RW, Amdur RJ, Morris CG, Kirwan J, Mendenhall WM. Definitive radiotherapy in the management of paragangliomas arising in the head and neck: a 35-year experience. Head Neck 2008;30(11):1431–1438.
68. Forest JA 3rd, Jackson CG, McGrew BM. Long-term control of surgically treated glomus tympanicum tumors. Otol Neurotol 2001;22(2):232–236.
69. Sajid MS, Hamilton G, Baker DM; Joint Vascular Research Group. A multicenter review of carotid body tumour management. Eur J Vasc Endovasc Surg 2007;34(2):127–130.
70. Jackson RS, Myhill JA, Padhya TA, McCaffrey JC, McCaffrey TV, Mhaskar RS. The effects of preoperative embolization on carotid body paraganglioma surgery: a systematic review and meta-analysis. Otolaryngol Head Neck Surg 2015;153(6):943–950.
71. Gilbo P, Morris CG, Amdur RJ, et al. Radiotherapy for benign head and neck paragangliomas: a 45-year experience. Cancer 2014;120(23):3738–3743.
72. Ivan ME, Sughrue ME, Clark AJ, et al. A meta-analysis of tumor control rates and treatment-related morbidity for patients with glomus jugulare tumors. J Neurosurg 2011;114(5):1299–1305.
73. Niemeijer ND, Alblas G, van Hulsteijn LT, Dekkers OM, Corssmit EP. Chemotherapy with cyclophosphamide, vincristine and dacarbazine for malignant paraganglioma and pheochromocytoma: systematic review and meta-analysis. Clin Endocrinol (Oxf) 2014;81(5):642–651.
74. Fishbein L, Ben-Maimon S, Keefe S, et al. *SDHB* mutation carriers with malignant pheochromocytoma respond better to CVD. Endocr Relat Cancer 2017;24(8):L51–L55.
75. Hadoux J, Favier J, Scoazec JY, et al. SDHB mutations are associated with response to temozolomide in patients with metastatic pheochromocytoma or paraganglioma. Int J Cancer 2014;135(11):2711–2720.
76. Breen W, Bancos I, Young WF Jr, et al. External beam radiation therapy for advanced/unresectable malignant paraganglioma and pheochromocytoma. Adv Radiat Oncol 2017;3(1):25–29.
77. Fishbein L, Bonner L, Torigian DA, et al. External beam radiation therapy (EBRT) for patients with malignant pheochromocytoma and non-head and -neck paraganglioma: combination with 131I-MIBG. Horm Metab Res 2012;44(5):405–410.
78. Pryma DA, Chin BB, Noto RB, et al. Efficacy and safety of high-specific-activity ^{131}I-MIBG therapy in patients with advanced pheochromocytoma or paraganglioma. J Nucl Med 2019;60(5):623–630.
79. Strosberg J, El-Haddad G, Wolin E, et al. Phase 3 trial of ^{177}Lu-Dotatate for midgut neuroendocrine tumors. N Engl J Med 2017;376(2):125–135.
80. Zandee WT, Feelders RA, Smit Duijzentkunst DA, et al. Treatment of inoperable or metastatic paragangliomas and pheochromocytomas with peptide receptor radionuclide therapy using 177Lu-DOTATATE. Eur J Endocrinol 2019;181(1):45–53.
81. Satapathy S, Mittal BR, Bhansali A. 'Peptide receptor radionuclide therapy in the management of advanced pheochromocytoma and paraganglioma: A systematic review and meta-analysis'. Clin Endocrinol (Oxf) 2019;91(6):718–727.
82. Rednam SP, Erez A, Druker H, et al. Von Hippel-Lindau and hereditary pheochromocytoma/paraganglioma syndromes: clinical features, genetics, and surveillance Recommendations in Childhood. Clin Cancer Res 2017;23(12):e68–e75.
83. Amar L, Pacak K, Steichen O, et al. International consensus on initial screening and follow-up of asymptomatic SDHx mutation carriers. Nat Rev Endocrinol 2021;17(7):435–444.